



Article

Improved One- and Multiple-Photon Excited Photoluminescence from Cd²⁺-Doped CsPbBr₃ Perovskite NCs

Ivan D. Skurlov ¹, Wenxu Yin ², Azat O. Ismagilov ³, Anton N. Tcypkin ³, Haohang Hua ², Haibo Wang ², Xiaoyu Zhang ^{2,*}, Aleksandr P. Litvin ^{1,3,*} and Weitao Zheng ²

¹ Laboratory of Optics of Quantum Nanostructures, ITMO University, 197101 St. Petersburg, Russia; sky_id@itmo.ru

² Key Laboratory of Automobile Materials, College of Materials Science and Engineering, Jilin University, Changchun 130012, China; wenyuyin0108@163.com (W.Y.); huahaohang0520@163.com (H.H.); wanghaibo@jlu.edu.cn (H.W.); wtzheng@jlu.edu.cn (W.Z.)

³ Laboratory of Quantum Processes and Measurements, ITMO University, 197101 St. Petersburg, Russia; ismagilov.azat@itmo.ru (A.O.I.); tscypkin@itmo.ru (A.N.T.)

* Correspondence: zhangxiaoyu@jlu.edu.cn (X.Z.); litvin@itmo.ru (A.P.L.)

Abstract: Metal halide perovskite nanocrystals (NCs) attract much attention for light-emitting applications due to their exceptional optical properties. More recently, perovskite NCs have begun to be considered a promising material for nonlinear optical applications. Numerous strategies have recently been developed to improve the properties of metal halide perovskite NCs. Among them, B-site doping is one of the most promising ways to enhance their brightness and stability. However, there is a lack of study of the influence of B-site doping on the nonlinear optical properties of inorganic perovskite NCs. Here, we demonstrate that Cd²⁺ doping simultaneously improves both the linear (higher photoluminescence quantum yield, larger exciton binding energy, reduced trap states density, and faster radiative recombination) and nonlinear (higher two- and three-photon absorption cross-sections) optical properties of CsPbBr₃ NCs. Cd²⁺ doping results in a two-photon absorption cross-section, reaching 2.6×10^6 Goeppert-Mayer (GM), which is among the highest reported for CsPbBr₃ NCs.

Keywords: perovskite; nanocrystal; doping; nonlinear optical properties; photoluminescence; two-photon absorption



Citation: Skurlov, I.D.; Yin, W.; Ismagilov, A.O.; Tcypkin, A.N.; Hua, H.; Wang, H.; Zhang, X.; Litvin, A.P.; Zheng, W. Improved One- and Multiple-Photon Excited Photoluminescence from Cd²⁺-Doped CsPbBr₃ Perovskite NCs. *Nanomaterials* **2022**, *12*, 151. <https://doi.org/10.3390/nano12010151>

Academic Editor: Marcin Runowski

Received: 29 November 2021

Accepted: 29 December 2021

Published: 1 January 2022

Publisher's Note: MDPI stays neutral with regard to jurisdictional claims in published maps and institutional affiliations.



Copyright: © 2022 by the authors. Licensee MDPI, Basel, Switzerland. This article is an open access article distributed under the terms and conditions of the Creative Commons Attribution (CC BY) license (<https://creativecommons.org/licenses/by/4.0/>).

1. Introduction

Doping of cesium lead halide perovskites has become a novel approach to tuning their optoelectronic properties and enhancing their stability [1–4]. Doping may enhance their luminosity and promote charge carrier transport and crystal phase stabilization [2]. Different divalent metal ions including Mn²⁺, Sn²⁺, Ca²⁺, Zn²⁺, Cu²⁺, and Ni²⁺ have been used for isovalent B-site doping (where ABX₃ is a general structural formula) of cesium lead halide perovskite nanocrystals (NCs) [5–17]. B-site doping is also considered a new approach to achieving better characteristics of devices based on perovskite NCs, and that was demonstrated for CsPbBr₃ NCs, which are important nanomaterials to produce green-emitting light-emitting diodes (LEDs) [12–17]. Recently, the doping of CsPbBr₃ NCs with Mn²⁺ [18], Sn²⁺ [19], Ce³⁺ [20], Rb⁺ [21], and Co²⁺ [22] has been used to enhance the external quantum efficiency (EQE) and maximum luminance of the LEDs. Moreover, the doping may facilitate better environmental stability of the device [18] and optimization of the energy band diagram [23].

Metal halide perovskites can now be considered a new platform for nonlinear optics [24]. For instance, they demonstrate enormous values of nonlinear absorption cross-sections. The study of the processes involving simultaneous absorption of multiple

photons is of great importance for numerous applications, including high-resolution microscopy [25,26] and biomedical imaging [27,28]. Despite the great practical interest in these processes, their utilization is limited due to the lack of highly efficient nonlinear materials, and the employment of perovskites in this field is of tremendous importance. B-site doping is considered to be an effective tool for the further optimization of nonlinear optical responses from metal halide perovskite NCs [29,30]; however, very few reports have been published on this topic. Ketavath et al., recently showed that 0.08–0.1% Ni²⁺ doping of 2D CsPbBr₃ NCs induced a ~2.5-fold increase in the two-photon absorption (2PA) cross-section [31]. He et al., studied the influence of Mn²⁺ doping on the nonlinear optical properties of CsPbCl₃ NCs [32] and nanoplatelets (NPLs) [33]. They reported the wavelength-dependent 2PA cross-section of Mn²⁺-doped CsPbCl₃ NCs with a maximum value up to $\sim 3.2 \times 10^5$ GM (1 GM = 10^{-50} cm⁻⁴ s photon⁻¹) [32].

Cd²⁺ doping is an important example of engineering of perovskite NC properties. Cd²⁺ doping of CsPbBr₃ NCs was first reported by van der Stam and co-workers, who proposed a post-synthetic cation exchange reaction to replace some of the Pb²⁺ cations [11]. They showed that the doping caused a blue shift of optical transitions, induced by lattice contraction, while preserving a high photoluminescence quantum yield (PLQY) and narrow full width at half maximum (FWHM) of the PL band. A similar observation was recently made by Zhao et al., who synthesized Cd²⁺ doped CsPbBr₃ NCs inside a borosilicate glass matrix [34]. As an alternative approach, Mondal and co-workers demonstrated the post-synthetic treatment of CsPbCl₃ NCs with CdCl₂ that resulted in the tremendous growth of PLQY [35]. Very recently, Xie et al., demonstrated that post-synthetic surface treatment of CsPbBr₃ NCs with CdX₂ precursors enlarged their PLQY from 85% to 92% [36].

Although these results point to the undeniable effect of Cd²⁺ doping on all-inorganic NC optical properties, there is no information regarding its influence on their nonlinear optical properties. Here, we developed methods for obtaining Cd²⁺-doped perovskite NCs by direct synthesis using a mixture of PbBr₂ and CdBr₂ precursors. The investigation of the temperature dependencies of the PL responses allowed us to reveal additional features induced by Cd²⁺ doping. For the first time, we demonstrate that Cd²⁺ doping modifies nonlinear optical responses of CsPbBr₃ NCs: Cd²⁺ doped CsPbBr₃ NCs demonstrated bright one- and multi-photon excited emission, while a two-photon absorption cross-section reached 2.6×10^6 GM. First, we describe the influence of doping on the structural and linear optical properties of CsPbBr₃ NCs that allow the fabrication of an LED with a maximum luminance of 24,221 cd·m⁻², and then we demonstrate the improvement of nonlinear optical responses studied by means of two- and three-photon excited photoluminescent spectroscopy.

2. Materials and Methods

Materials. Lead bromide (PbBr₂, 99%), cesium carbonate (Cs₂CO₃, 99.95%), octadecene (ODE, 90%), oleic acid (OA, 90%), cadmium bromide tetrahydrate (CdBr₂·4H₂O, 98%), and oleylamine (OlAm, 80–90%) were purchased from Aladdin (Shanghai, China). Hexane, ethanol, and acetone were purchased from Sinopharm Chemical Reagent Co., Ltd. (Shanghai, China). Poly(3,4-ethylenedioxythiophene): polystyrene sulphonate (PEDOT:PSS), Poly[bis(4-phenyl) (4-butylphenyl) amine] (Poly-TPD) and 2,2',2''-(1,3,5-Benzinetriyl)-tris(1-phenyl-1-Hbenzimidazole) (TPBi) were purchased from Xi'an Polymer (Xi'an, Shannxi, China). Lithium fluoride (LiF) was purchased from Lumtec (New Taipei City, Taiwan).

Preparation of cesium oleate (Cs-OA) solution. In brief, Cs₂CO₃ (0.814 g), OA (2.5 mL), and ODE (30 mL) were loaded into a 100 mL three-neck flask. The flask was degassed at 120 °C for 60 min and then switched to N₂ flow. Finally, the flask was heated up to 150 °C until the Cs₂CO₃ completely dissolved.

Preparation of CsPbBr₃ and CsPb_{0.78}Cd_{0.22}Br₃ NCs. Briefly, PbBr₂ (0.376 mmol) and ODE (10 mL) were added to a 50 mL three-neck round bottom flask. The solution was degassed at 120 °C for 60 min under vacuum and then switched to N₂ flow. After injection of OA (1 mL) and OlAm (1 mL) the temperature was increased to 180 °C. Subsequently,

as-synthesized Cs-OA (1 mL) was promptly injected to the flask. After 5 s, an ice bath was used to stop the reaction. CsPb_{0.78}Cd_{0.22}Br₃ NCs were synthesized by adding 0.188 mmol of CdBr₂·4H₂O at the beginning of reaction while keeping the rest of the protocol intact.

Purification. First, the crude solution was purified by centrifugation at 5000 RPM for 10 min; the supernatant was discarded, and the precipitate was re-dispersed in hexane to form stable colloidal solutions. Second, ethyl acetate was introduced into the colloidal solutions at a volume ratio of 1:1, and then the mixture was centrifuged for 10 min at 10,000 RPM. Lastly, the final precipitate was dispersed in 2 mL hexane for LED fabrication.

LED fabrication. Glass substrates coated with indium tin oxide (ITO) were first sonicated consecutively with ethanol and acetone for 20 min each. To increase the work function, ITO substrates were treated with UV-ozone for 15 min. Then, PEDOT: PSS (25 nm thickness) was spin-coated on the ITO substrates at a speed of 4000 RPM for 40 s and then annealed at 150 °C for 15 min in ambient air. Subsequently, these substrates were transferred into a glovebox. The Poly-TPD solution (dissolved in chlorobenzene, 8 mg/mL, 30 nm) was spin coated onto the PEDOT: PSS film at a speed of 4000 RPM for 40 s and annealed at 150 °C for 15 min. The washed CsPb_{0.78}Cd_{0.22}Br₃ NCs (~35 nm thickness) were spin coated onto the Poly-TPD film at 1500 RPM for 40 s. Finally, TPBi (18 nm), LiF, and Al (LiF/Al, 55 nm) electrodes were deposited by thermal evaporation in a vacuum deposition chamber of $\sim 3 \times 10^{-6}$ Torr.

Characterization. UV-VIS absorption was measured using a Shimadzu UV-1800 (Shimadzu corporation, Kyoto, Japan) spectrophotometer. A JEM-2100F (JEOL Ltd., Tokyo, Japan) transmission electron microscope (TEM) was used to analyze the morphology of the NCs. X-ray diffraction (XRD) patterns were acquired using a Bruker D8 Advance X diffractometer (Cu K α , $\lambda = 1.5406$ Å). X-ray Photoelectron Spectroscopy (XPS) was performed on an ESCALAB 250 (Thermo Fisher Scientific Inc., Waltham, MA, USA) spectrometer with a mono X-Ray source Al K α excitation (1486.6 eV). Ultraviolet photoelectron spectra (UPS) were collected using a PREVAC (PREVAC, Rogów, Poland) system. A Keithley 2400 (Keysight technologies, Santa Rosa, CA, USA) source meter and a PR-750 Spectroradiometer (Photo Research Inc., Chatsworth, CA, USA) were used to acquire the current density–luminance–voltage (J-V-L) characteristics. The molar concentration of the nanocrystals in the solution was obtained from the absorption spectra; see Appendix A for details.

PL spectroscopy. PL spectra were measured using a custom-built setup based on an Acton-2500 monochromator equipped with an Andor iDus 401A CCD camera (Andor Technology Ltd., Belfast, Northern Ireland) [37–39]. To avoid any thermal effects, the samples were excited with unfocused 80 μ W 405 nm laser (Lasever Inc., Ningbo, China) excitation passed through a 0.8 mm diaphragm. The obtained spectra were corrected using the blackbody radiation source (Thorlabs SLS201/M, Thorlabs, Newton, NJ, USA). For the measurements at decreased temperatures, NCs were added to 8 wt% PMMA solution in toluene under an inert atmosphere and were left stirring for 1 h at 1000 RPM. The solution was dropped onto a pre-cleaned glass substrate and spin-coated at 2000 RPM. The optical density of the films did not exceed 0.1 at 400 nm. The samples were transferred to a Linkam THMS600 Microscope Stage cryostat (Linkam scientific instruments, Tadworth, UK). For the transient measurements, a MicroTime 100 microscope (PicoQuant, Berlin, Germany) employing time-correlated single-photon counting was used. The microscope was equipped with 3 \times objective lens and a 50 ps pulse diode laser head operated at 405 nm. PL lifetimes were found to be dependent on the excitation power density, as was previously reported [40]. The excitation power density was maintained below the value at which the dependence of PL lifetimes on excitation intensity occurred. The IRF was measured and deconvoluted from the decay curves. After the deconvolution, the PL decays were fitted by the 3-exponential decay law.

2-photon excited PL measurements. Nanocrystals were dispersed in toluene in 1-mm-thick optical glass cuvettes. Two-photon PL was excited using an Avesta femtosecond laser system (Avesta project Ltd., Troitsk, Moscow, Russia) with a peak center at 800 nm, pulse width of ~ 30 fs, 1 kHz repetition rate, and power density ranging from 0.035 W/cm² to

1.150 W/cm². PL was detected using a USB4000-UV-VIS-ES (Ocean Insight, Largo, FL, USA) spectrometer [41]. The obtained spectra were corrected using the blackbody radiation source (Thorlabs SLS201/M, Thorlabs, Newton, NJ, USA). Rhodamine 6G in ethanol was used as a standard for the 2PA cross-section calculation. Rhodamine 6G cross-section was taken to be $128 \pm 84 \text{ GM}$ ($10^{-50} \text{ cm}^{-4} \cdot \text{s} \cdot \text{photon}^{-1}$) [42–44]. A detailed description of the two-photon excited PL analysis can be found in Appendix B.

3-photon excited PL measurements. An optical parametric amplifier (OPA-TOPAS, Light Conversion, Vilnius, Lithuania) was used as an excitation source for the generation of 3-photon excited PL from perovskite NC solutions in toluene. The femtosecond pump radiation from a regenerative Ti-sapphire amplifier (pulse duration 35 fs, energy 2.2 mJ, 1 kHz repetition rate, 800 nm central wavelength) was used as a pump radiation for OPA. Optical radiation from OPA in the range 1300–1560 nm and under a pulse duration of 60 fs passed through quartz cuvette with sample solutions. The diameter of the laser beam was 5 mm, and the excitation power density varied from 0.35 W/cm² to 1.52 W/cm². To measure the dependence of the integrated PL intensity vs. power density, the excitation wavelength was fixed at 1300 nm, and an optical attenuator with neutral filters was used to change the excitation power. For the wavelength-dependent measurements, the pulse energy was fixed at $250 \pm 20 \mu\text{J}$. The PL signal was detected using a USB4000-UV-VIS-ES (Ocean Insight, Largo, FL, USA) spectrometer. 3PA absorption cross-section was calculated analogous to the two-photon excitation (see Appendix B for the details) with Rhodamine 6G in ethanol as a reference (3PA cross section of $3 \times 10^{-80} \text{ cm}^6 \text{ s}^2$ [45]).

3. Results

3.1. Synthesis and Characterization of NCs

The morphology and crystal structure of the as-synthesized CsPbBr₃ NCs and Cd²⁺-doped CsPbBr₃ (CsPb_{0.78}Cd_{0.22}Br₃, the element content was confirmed by X-ray photoelectron spectroscopy) NCs were investigated by transmission electron microscopy (TEM). As shown in Figure 1a,d, the TEM image of CsPb_{0.78}Cd_{0.22}Br₃ NCs exhibited a more uniform morphology and narrower size distribution than CsPbBr₃ NCs, as clearly seen from the particle size distribution histograms (Figure 1c,f). Both samples were highly crystalline, which can be confirmed by the ordered crystal lattices in high-resolution TEM (HRTEM) images of Figure 1e. The obvious lattice fringes were identified to be 5.8 and 5.7 Å, which is in good agreement with the (100) crystal facets of the CsPbBr₃ cubic phase. As for the reduction in lattice spacing in CsPb_{0.78}Cd_{0.22}Br₃ NCs, it can be attributed to the lattice contraction derived from the Cd²⁺ doping. To further characterize the crystal structure, we measured X-ray diffraction patterns (XRD); the results are presented in Figure 1g. The two main peaks located at ~14.8° and 30.2° were assigned to the (100) and (200) planes of CsPbBr₃ cubic phase, respectively. In contrast to CsPbBr₃ NCs, the characteristic peaks of CsPb_{0.78}Cd_{0.22}Br₃ NCs showed an obvious shift to higher angles without introducing any extra peaks, which indicates that the Cd²⁺ incorporation did not change the crystal structure but only contracted the lattice spacing, corresponding to the HRTEM results. To verify the effect on optical properties, the absorption spectra of these samples were measured and are summarized in Figure 1h. The characteristic absorption peak shifted from 501 nm to 495 nm after Cd²⁺ doping, and the absorption largely decreased in the 520–600 nm range, indicating the reduction of the trap state density in CsPb_{0.78}Cd_{0.22}Br₃ NCs.

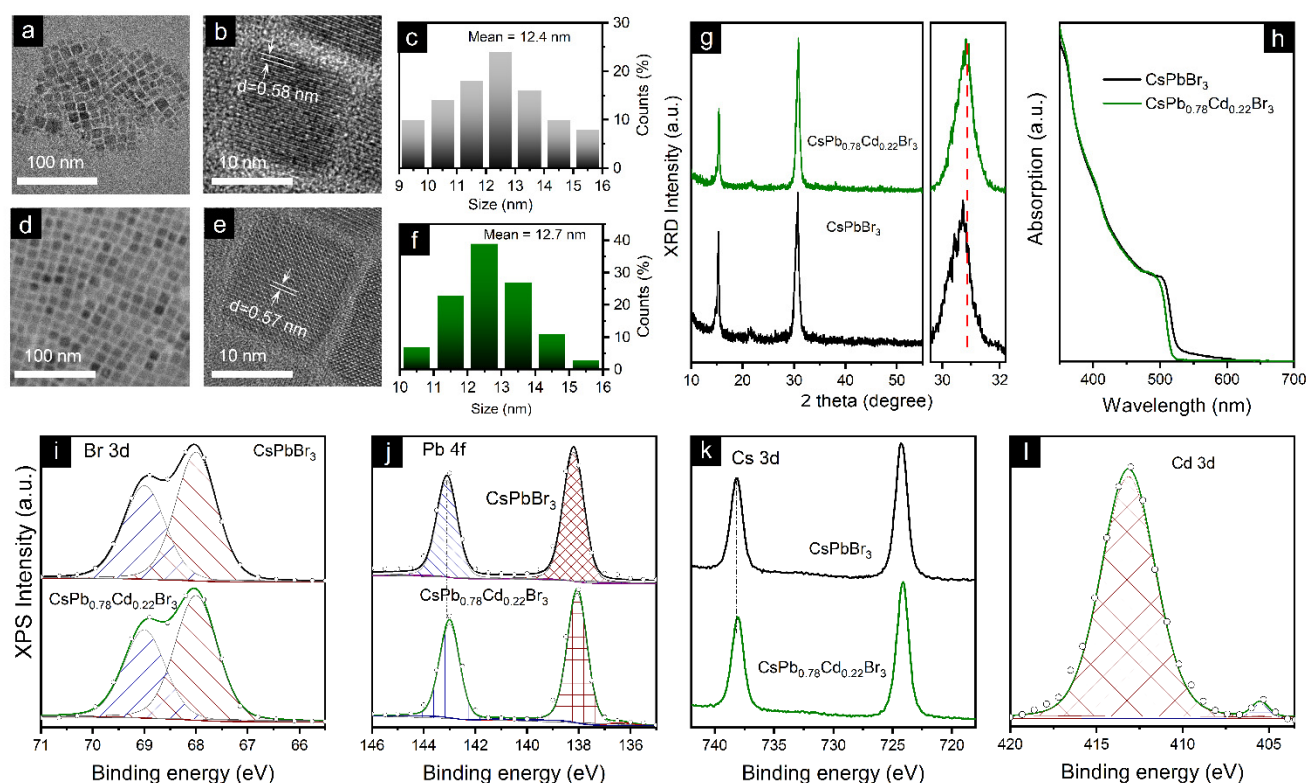


Figure 1. TEM images of (a) CsPbBr₃ and (d) CsPb_{0.78}Cd_{0.22}Br₃ NCs; their corresponding HR-TEM images are exhibited in (b,e). (c,f) are particle size distribution histograms of CsPbBr₃ and CsPb_{0.78}Cd_{0.22}Br₃ NCs; their corresponding XRD patterns and UV–vis absorption spectra are shown in (g,h), respectively. (i–l) XPS spectra for the (a) Br, (b) Pb, (c) Cs, and (d) Cd elements collected for the CsPbBr₃ and CsPb_{0.78}Cd_{0.22}Br₃ NCs.

To identify the influence of Cd²⁺ doping on the chemical states of constituting elements in the perovskite NC film, we performed X-ray photoelectron spectroscopy (XPS) measurements of CsPbBr₃ and CsPb_{0.78}Cd_{0.22}Br₃ NC films. Figure 1i–l shows XPS spectra for the Br, Pb, Cs, and Cd elements, respectively, all calibrated with C 1 s. No peak shift was observed for Br 3d, while the Pb 4f and Cs 3d peaks shifted to higher binding energy in the CsPb_{0.78}Cd_{0.22}Br₃ NC film compared to the CsPbBr₃ NC film. The result is consistent with the crystal lattice contraction observed in the HRTEM images and XRD patterns. As expected, CsPb_{0.78}Cd_{0.22}Br₃ NC films demonstrated a noticeable Cd 3d peak, and the elemental ratio of Cd:Pb was around 0.29:1.

3.2. One-Photon Excited PL

The PL spectra for CsPbBr₃ (black) and CsPb_{0.78}Cd_{0.22}Br₃ (green) NCs in toluene are shown in Figure 2a. The Cd²⁺ doping induced a 25-meV blue shift of the PL peak position. The blue shift of PL peak position and absorption onset (Figure 1h) are typical for the doping of perovskite NCs by guest cations with smaller ionic radii [3]. The measured change of the bandgap fitted well with the theoretical predictions reported by Navas et al., for Cd²⁺-doped MAPbI₃ NCs [46]. Van der Stam et al. [11] recently demonstrated that introducing smaller cations, including Cd²⁺, induced a parent NC lattice contraction. A small shift of the band-edge emission was recently observed for Cd²⁺-doped CsPbCl₃ NCs [47], which indicates that Cd²⁺ ions diffuse into the NC volume rather than passivate their surface. Both spectra shown in Figure 2a had similar FWHMs, i.e., 90 and 91 meV. After the Cd²⁺ doping, the PLQY increased from 75% to 90%. The PL decay for pristine and doped NCs is shown in Figure 2b. The decay curves were fitted by a 3-exponential function. The averaged PL lifetime decreased from 18 ± 2 to 9.0 ± 0.5 ns after the doping, which corresponds well with the data obtained by Van der Stam et al., for Cd²⁺-doped CsPbBr₃

NCs [11]. Since we observed both a decrease in the PL decay time and an increase in the PLQY, this points to an increase in the radiative recombination rate and not the appearance of additional fast nonradiative recombination channels.

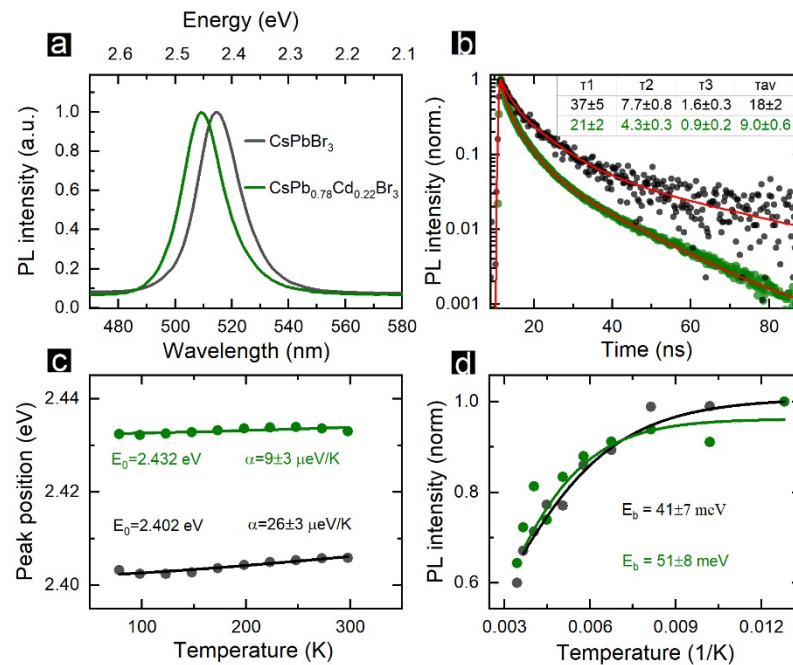


Figure 2. One-photon excited PL from CsPbBr₃ (black) and CsPb_{0.78}Cd_{0.22}Br₃ (green) NCs. (a) PL spectra recorded under 405 nm laser excitation. (b) PL decay curves recorded under pulsed 405 nm laser excitation; red lines show 3-exponential fitting, and the estimated decay times constants are listed in the table along with the average PL decay times. (c) Temperature dependencies of the PL peak position; solid lines show Varshni fitting. (d) Temperature dependencies of integrated PL intensity; solid lines show Arrhenius-type fitting.

The analysis of the temperature dependencies of PL spectra revealed more differences between the pristine and doped NCs. Figure 2 shows the temperature dependencies of the PL peak positions and their approximation with a Varshni function (Equation (1)) [48].

$$E_G(T) = E_{G0} - \alpha \frac{T^2}{T + \beta}, \quad (1)$$

where E_{G0} is the bandgap (PL peak position) at 0 K, α is the coefficient of the temperature shift, and β is the Debye temperature, i.e., 224.8 K [49]. The peak position temperature shift coefficient α was $26 \pm 3 \mu\text{eV/K}$ for CsPbCl₃ NCs, which is almost an order smaller than that reported in Refs. [40,50,51]. Since many physical mechanisms contribute to a temperature shift of the bandgap for nanosized semiconductors, many factors may influence the determined α value, and the reports for different synthetic procedures may vary in a wide range [52]. The CsPb_{0.78}Cd_{0.22}Br₃ NCs demonstrated an even smaller α value, $9 \pm 3 \mu\text{eV/K}$. Such a negligible temperature shift of the PL band is beneficial for the development of LEDs with stable color purity [53]. Both types of NCs demonstrated an increase in PL intensity with a temperature decrease (Figure 2d). Fitting the integrated PL intensity vs. temperature with Arrhenius-type equation (Equation (2)) allowed us to determine the exciton binding energy (E_b) in perovskite NCs [54].

$$I_{PL} = \frac{I_0}{(1 + A \times e^{-\frac{E_b}{k_B T}})} \quad (2)$$

where I_0 is the integrated PL intensity at 0 K, k_B is the Boltzmann constant, and E_b is the binding energy. E_b was 41 ± 7 meV for the pristine CsPbBr₃ NCs. This value is very close to those recently determined by Yuan et al., using the same experimental approach [51] and estimated by Protesescu et al., within the effective mass approximation [55]. The CsPb_{0.78}Cd_{0.22}Br₃ NCs had a higher E_b value, 51 ± 8 meV, which makes them attractive candidates to be used in perovskite-based LEDs [56,57].

3.3. LEDs

To demonstrate their practical applicability, the CsPb_{0.78}Cd_{0.22}Br₃ NCs were adopted as emitters to fabricate LEDs. The lowest unoccupied molecular orbital (LUMO) and the highest occupied molecular orbital (HOMO) were determined by the ultraviolet photoelectron spectroscopy (UPS, Figure 3a) of CsPb_{0.78}Cd_{0.22}Br₃ NC film [58]. The Tauc plot of the CsPb_{0.78}Cd_{0.22}Br₃ NC film (Figure 3b) revealed a bandgap of 2.41 eV [59]. Thus, the LUMO and HOMO values of CsPb_{0.78}Cd_{0.22}Br₃ NCs were confirmed to be -3.07 and -5.48 eV, respectively. The conventional multilayered LED was fabricated using patterned indium–tin oxide (ITO) as the anode, poly(ethylenedioxythiophene):polystyrenesulfonate (PEDOT:PSS, 25 nm) film and poly(*N,N'*-bis(4-butylphenyl)-*N,N'*-bis(phenyl)-benzidine) (poly-TPD, 40 nm) film as the hole transporting layer (HTL), CsPb_{0.78}Cd_{0.22}Br₃ NC film (40 nm) as the emitting layer, 1,3,5-tris(*N*-phenylbenzimidazol-2-yl) benzene (TPBi, 40 nm) film as the electron-transporting layer (ETL), and LiF/Al as the cathode. The energy band diagram for all functional layers of LED is given in Figure 3c. Figure 3d demonstrates the current density–voltage (J–V) and luminance–voltage (L–V) curves of the LEDs, which showed a peak luminance of $24,221 \text{ Cd}\cdot\text{m}^{-2}$ under the working bias of 7.0 V. The peak EQE of 10.6% was achieved at 0.3 mA cm^{-2} (inset of Figure 3d). Normalized PL and electroluminescence (EL) spectra of a typical LED are given in Figure 3e. Apparently, the EL originated from CsPb_{0.78}Cd_{0.22}Br₃ NCs without noticeable contribution from any charge transport layers, indicating that the perovskite NCs served as the exciton recombination centers for the device, and a balanced charge transport was achieved. The device PL and EL both exhibited emission peaks at 511 nm. The inset of Figure 3e is the image of a working LED.

3.4. Multiphoton-Induced PL

Two-photon excited PL spectra of perovskite NCs were recorded using non-resonant 800 nm laser excitation. To estimate the type of multi-photon process, we measured NC PL spectra with different excitation power densities. Figure 4a–c demonstrates the log–log plots of integrated PL intensity vs. excitation power density for the Rhodamine 6G (used as a reference), CsPbBr₃ NCs, and CsPb_{0.78}Cd_{0.22}Br₃ NCs, respectively. Nearly quadratic dependencies of integrated PL intensity vs. power density clearly indicate the two-photon absorption (2PA) process [60]. At higher excitation power density, the integrated 2PA-excited PL intensity demonstrated a saturation-like behavior as previously reported for the MAPbBr₃ films [61] and 2D (PEA)₂PbI₄ perovskites [62]. We can attribute this observation to the influence of strong laser radiation exposure, which can lead to perovskite NC partial destruction caused by heating. It should also be noted that CsPb_{0.78}Cd_{0.22}Br₃ NCs showed a smaller deviation from the theoretical power law, which may indicate their improved stability under laser radiation.

The 2PA absorption cross-sections were calculated using Rhodamine 6G as a standard (see experimental section and Appendix B). The reported NC values of third-order nonlinear optical parameters strongly depend on their stoichiometry [63], size [64], and shape [65]. The value obtained for the pristine CsPbBr₃ NCs $(3.2 \pm 1.9) \times 10^5 \text{ GM}$ was very close to those recently reported (see Table 1) [64–68]. CsPb_{0.78}Cd_{0.22}Br₃ NCs demonstrated an almost one-order enhanced value of the 2PA cross-section, and the obtained value is among the highest reported for CsPbBr₃ NCs [69,70].

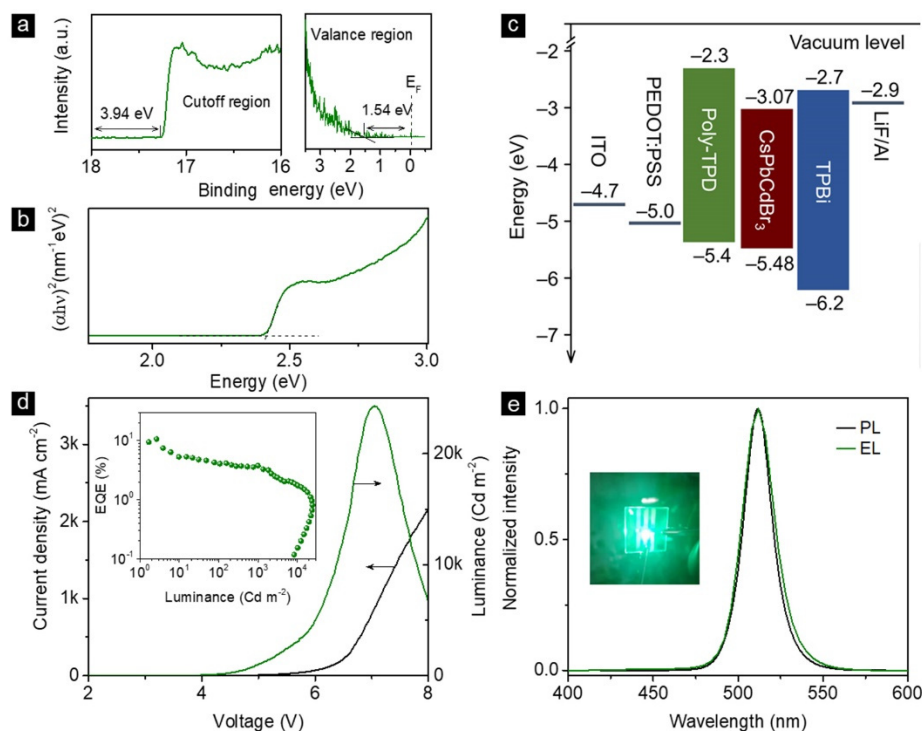


Figure 3. (a) UPS spectra for the cutoff (left) and valence (right) regions and (b) Tauc plot of the CsPb_{0.78}Cd_{0.22}Br₃ NCs film; (c) overall energy band diagram of the CsPb_{0.78}Cd_{0.22}Br₃ NC-based LED, (d) current density and brightness vs. driving voltage of the CsPb_{0.78}Cd_{0.22}Br₃ NC-based LED, (e) normalized PL and EL spectra for CsPb_{0.78}Cd_{0.22}Br₃ NCs in the film and LEDs; the inset is a photograph of the working LED.

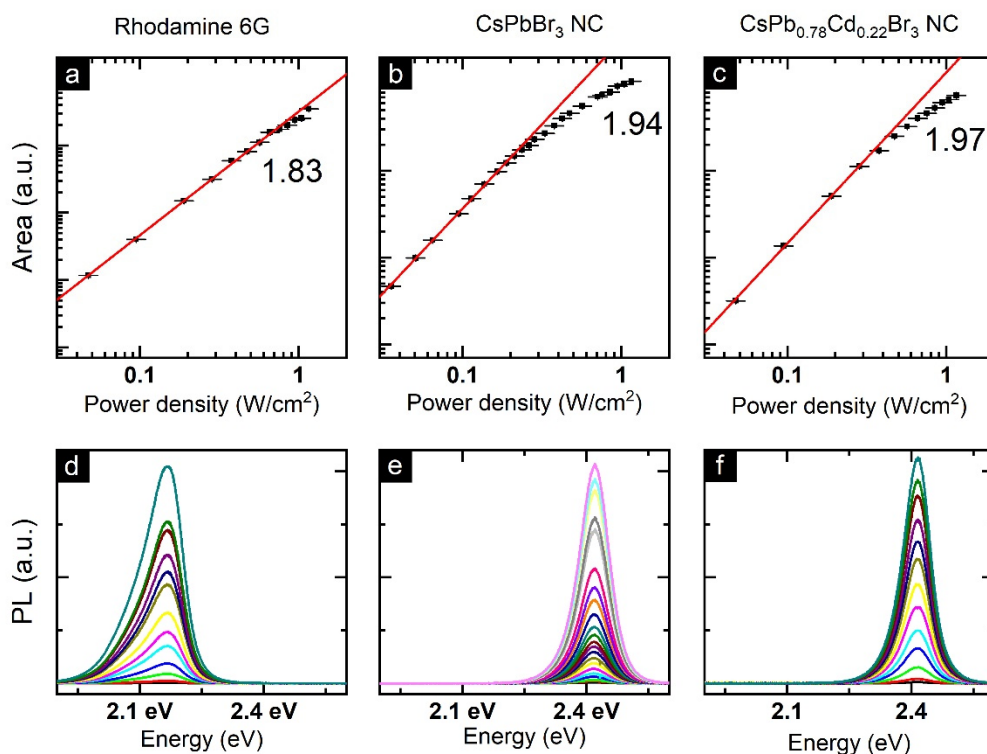


Figure 4. The log–log plots of integrated PL area vs. power density for Rhodamine 6G (a), CsPbBr₃ NCs (b), and CsPb_{0.78}Cd_{0.22}Br₃ NCs (c). (d–f) corresponding 2PA-excited PL spectra measured at different excitation power densities.

Table 1. Pristine and volume-normalized 2PA and 3PA cross-sections for the CsPbBr₃ NCs, nanoplatelets (NP), nanorods (NR), and nanowires (NW).

Sample	σ_{2PA} (GM)	Volume Normalized σ_{2PA} (GM/nm ³)	σ_{3PA} (10 ⁻⁸⁰ cm ⁶ s ² Photon ⁻²)	Volume Normalized σ_{3PA} (10 ⁻⁸⁰ cm ⁶ s ² Photon ⁻² nm ⁻³)	Ref.
CsPbBr ₃ NC 12.4 nm	$(3.2 \pm 1.9) \times 10^5$ (800 nm, 30 fs)	171 ± 112	$(1.7 \pm 1.0) \times 10^5$ (1300 nm, 30 fs)	89 ± 18	This work
CsPb _{0.78} Cd _{0.22} Br ₃ NC 12.7 nm	$(2.6 \pm 0.8) \times 10^6$ (800 nm, 30 fs)	1265 ± 830	$(2.1 \pm 0.7) \times 10^5$ (1300 nm, 30 fs)	102 ± 21	This work
CsPbBr ₃ NC 7.3 nm	1.2×10^5 (720 nm 100 fs)	308	2.8×10^4 (1200 nm 100 fs)	72	[68]
CsPbBr ₃ NP	2.28×10^5 (720 nm 100 fs)	1562	1.05×10^5 (1200 nm 100 fs)	720	[68]
CsPbBr ₃ NC 9 nm	2×10^6 (800 nm 100 fs)	2743	1.0×10^6 (1200 nm 100 fs)	1372	[71]
CsPbBr ₃ NC 7 nm	1.8×10^5 (700–1000 nm 100 fs)	525	9.1×10^5 (1000–1500 nm 100 fs)	2653	[63]
CsPbBr ₃ NR	1.5×10^6 (800 nm 100 fs)	221	2.7×10^5 (1300 nm 100 fs)	40	[72]
CsPbBr ₃ NC 12 nm	9.8×10^5 (800 nm 50 fs)	567			[65]
CsPbBr ₃ NC 9 nm	1.2×10^5 (800 nm 100 fs)	164			[66]
CsPbBr ₃ NC 12.4 nm	2.2×10^5 (800 nm)	115			[67]
CsPbBr ₃ NC 9 nm	2.7×10^6 (800 nm 90 fs)	3704			[69]
CsPbBr ₃ NC 4.6 nm	1.6×10^4 (800 nm 120 fs)	164			[64]
CsPbBr ₃ NC 5.2 nm	2.9×10^4 (800 nm 120 fs)	206			[64]
CsPbBr ₃ NC 6.9 nm	6.1×10^4 (800 nm 120 fs)	186			[64]
CsPbBr ₃ NC 9.4 nm	1.8×10^5 (800 nm 120 fs)	217			[64]
CsPbBr ₃ NC 11.4 nm	4.55×10^5 (800 nm 120 fs)	307			[64]
CsPbBr ₃ NC 28 nm	8.1×10^4 (800 nm 100 fs)	4			[73]
CsPbBr ₃ NP	4.2×10^5 (800 nm 100 fs)	300			[73]
CsPbBr ₃ NW	2.3×10^5 (800 nm 100 fs)	12			[73]

To study the 5th-order nonlinear optical response, three-photon absorption (3PA)-induced PL was investigated using the wavelength-tunable excitation in the 1300–1560 nm spectral range. First, the excitation wavelength was fixed at 1300 nm, and the integrated PL intensity vs. excitation power dependencies for the pristine and doped perovskite NCs were measured (Figure 5a,c). For both samples, the dependencies were similar to a

cubic function, indicating the 3-photon excited process solely [74]. To calculate the 3PA cross-sections, Rhodamine 6G was used as a standard. Similar to the results obtained for the 2PA excited PL, the 3PA cross-section was higher for CsPb_{0.78}Cd_{0.22}Br₃ NCs (2.1 ± 0.7 vs. $1.7 \pm 1.0 \times 10^{-75}$ cm⁶ s² photon⁻²). Spectral tuning of the used excitation allowed us to obtain the wavelength-dependencies of the 3PA cross-section for the pristine CsPbBr₃ and doped CsPb_{0.78}Cd_{0.22}Br₃ NC (Figure 5b,d). For both samples, the wavelength dependencies of the 3PA cross-sections well matched the linear absorption spectra of the NC solutions, except the region of intense absorption of toluene (1340–1440 nm). This observation is in line with previously reported wavelength dependencies obtained for both 2PA and 3PA in CsPbBr₃ NCs [64,68].

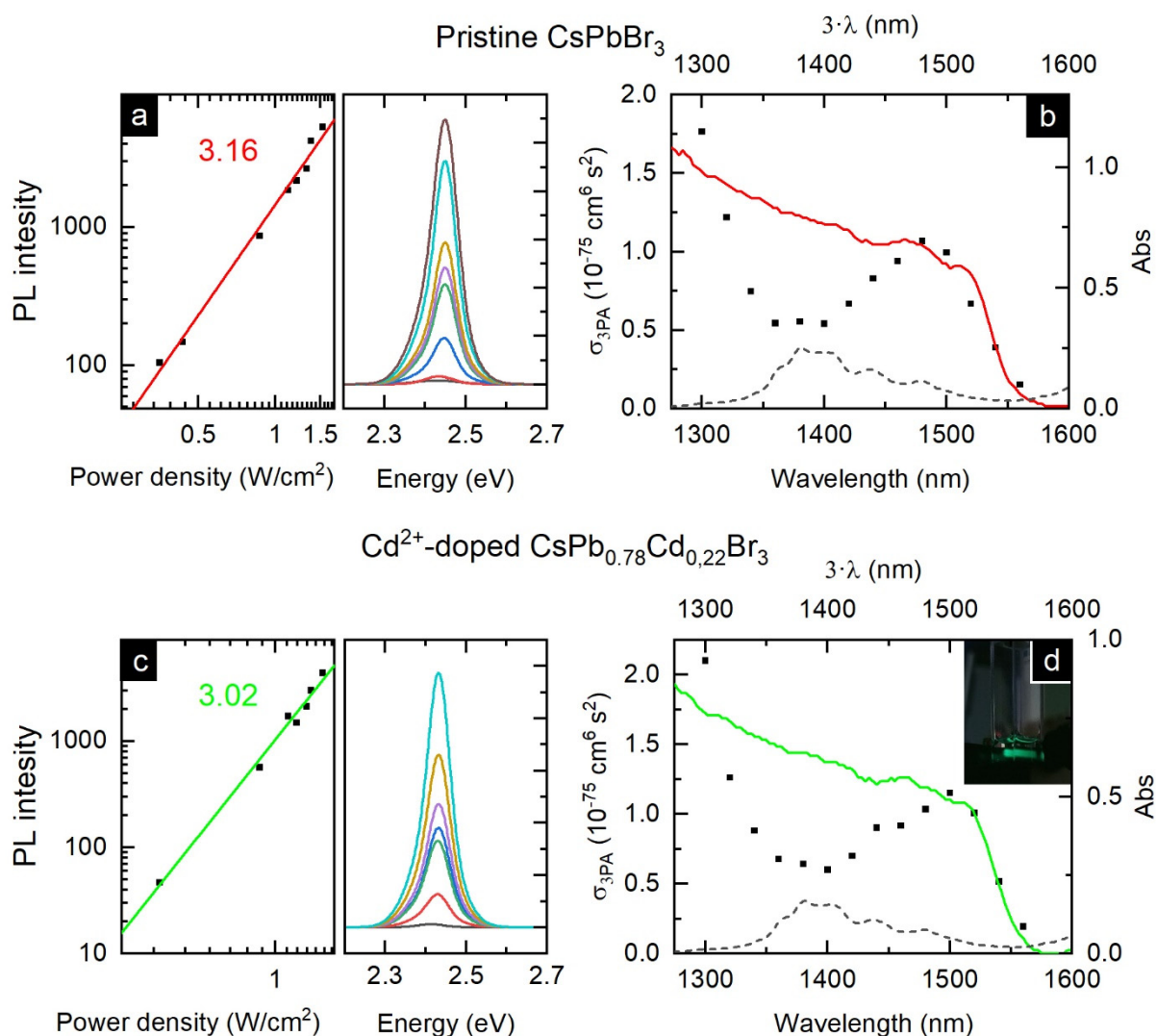


Figure 5. Three-photon excited photoluminescence of the studied NC. The log–log plots of the integrated PL area vs. power density for CsPbBr₃ NCs (a) and CsPb_{0.78}Cd_{0.22}Br₃ NCs (c). On the side are corresponding 3PA-excited PL spectra measured at different excitation power densities. 3PA absorption cross-section spectral dependencies for (b) CsPbBr₃ NCs and (d) CsPb_{0.78}Cd_{0.22}Br₃ NCs (on the inset is the photo of the PL from the CsPb_{0.78}Cd_{0.22}Br₃ NC solution when excited at 1560 nm). Dashed lines in (b,d) are the absorption of toluene at 1300–1600 nm, while colored lines show corresponding linear absorption drawn as a function of Abs(3·λ).

4. Conclusions

To conclude, we demonstrate that the engineering of the B-site in metal halide perovskite NCs has great potential for the improvement of their optical properties. Importantly,

we revealed that this strategy may induce a huge change in their nonlinear optical responses. The insertion of Cd^{2+} into CsPbBr_3 NCs resulted in an improvement of their morphological and optical properties, including greater exciton binding energy of 51 meV, reduced trap state density, faster radiative recombination, and high photoluminescence quantum yield reaching 90%. An even more significant improvement was associated with a change in the nonlinear optical response of the Cd^{2+} -doped CsPbBr_3 NCs. The TPA cross-section of 2.6×10^6 GM was evaluated, which is among the highest reported for CsPbBr_3 perovskite NCs. The findings demonstrate that the perovskite NCs with a rationally engineered B-site have great potential for light-emission and nonlinear optical applications.

Author Contributions: I.D.S. and W.Y. contributed equally. Conceptualization: A.P.L.; Investigation: I.D.S., W.Y., A.O.I., A.N.T., H.H., H.W., X.Z., A.P.L.; Project administration: A.P.L. and W.Z.; Visualization: I.D.S. and W.Y.; writing original draft: I.D.S. and W.Y.; writing review and editing: X.Z. and A.P.L.; Validation: W.Z. All authors have read and agreed to the published version of the manuscript.

Funding: The work was supported by the Russian Science Foundation (21-73-10131), the National Natural Science Foundation of China (52072141), the Natural Science Foundation of Jilin Province (Grant No. 20180101294JC), and the Fundamental Research Funds for the Central Universities (JLU, 1018320194002, 2019JCXK-31).

Data Availability Statement: All required data is provided within the manuscript.

Acknowledgments: A.P.L. thanks the Ministry of Education of the Russian Federation for the financial support (Scholarship of the President of the Russian Federation for young scientists and graduate students, SP-149.2021.1).

Conflicts of Interest: The authors declare no conflict of interest.

Appendix A. Calculation of Perovskite NC Molar Concentration

The perovskite NC extinction coefficient (ϵ) at 400 nm was calculated from the following equation:

$$\epsilon = \frac{D}{C_M l} = \frac{m_{NC} D}{C_{mass} l} = \frac{N_A \times V_{NC} \times \rho D}{C_{mass} l} \quad (\text{A1})$$

where D is the absorbance of the sample at 400 nm; C_M —NC molar concentration; l —cuvette length; m_{NC} —molar mass of the single NC; C_{mass} —mass concentration; N_A —the Avogadro number; V_{NC} —NC volume (determined from the known NC size); ρ —the NC density. NC density was calculated by normalizing the crystalline cell mass to the cell volume:

$$\rho = \frac{m_{cell}}{V_{cell}} = \frac{m_{cell}}{r^3} \quad (\text{A2})$$

where m_{cell} and V_{cell} are the respective cell mass and cell volume, r is the edge length, determined from TEM (see Figure 1). Cell mass was calculated from known NC stoichiometry. The resulting densities were 4.935 g/cm^3 for CsPbBr_3 and 5.012 g/cm^3 for $\text{CsPb}_{0.78}\text{Cd}_{0.22}\text{Br}_3$. Increased NC density in doped NCs arises from the lattice contraction observed from TEM (see Figure 1b,e). Mass concentration of the solution was determined from the weight of thoroughly washed and dried NCs.

The ϵ values for the CsPbBr_3 and $\text{CsPb}_{0.78}\text{Cd}_{0.22}\text{Br}_3$ NCs were $(3.63 \pm 0.18) \times 10^7 \text{ mol}^{-1}\text{cm}^{-1}$ and $(3.57 \pm 0.09) \times 10^7 \text{ mol}^{-1}\text{cm}^{-1}$, respectively. To verify the calculated extinction coefficients, we compared the values with the ones that were obtained for the pristine CsPbBr_3 using Equation (A3) [75].

$$\epsilon = 2.42 \times 10^4 \times d^3 (M \cdot \text{cm})^{-1} \quad (\text{A3})$$

where d is the edge length of the NCs in nanometers. The calculated value was $(4.46 \pm 0.22) \times 10^7 \text{ mol}^{-1}\text{cm}^{-1}$, which is fairly close to the values obtained from the aforementioned determination of extinction coefficients. Some difference may be caused by the overestimation of the NCs mass because some ligands still may remain at the NC surface. Using the deter-

mined mass absorption coefficient and NC molar weight, linear absorption cross-sections may be easily calculated. The linear absorption cross-sections were $4.94 \times 10^{-14} \text{ cm}^2$ and $4.86 \times 10^{-14} \text{ cm}^2$ for CsPbBr₃ and CsPb_{0.78}Cd_{0.22}Br₃ NCs, respectively. Recently, absorption cross-sections at 400 nm in the range of $1.3\text{--}3.4 \times 10^{-14} \text{ cm}^2$ were reported for CsPbBr₃ NCs with sizes of 6.2–9.3 nm, [76–79]; our values are similar and expectedly slightly higher due to a larger NC size. This supports the applicability of the estimated concentration for the correct measurements of multiphoton absorption cross-sections.

Concentrations of NCs and Rhodamine 6G were determined from Beer's law. For Rhodamine 6G, the known extinction coefficient ($\sim 40,000 \text{ mol}^{-1} \text{ cm}^{-1}$) at 500 nm was used. [80,81].

Appendix B. Multiphoton Absorption Cross-Section Calculation

Rhodamine 6G in ethanol was used as a standard for the 2PA cross-section calculation. The Rhodamine 6G cross-section was taken to be $128 \pm 84 \text{ GM}$ ($10^{-50} \text{ cm}^{-4} \cdot \text{s} \cdot \text{photon}^{-1}$), as averaged from the literature data (taken at 800 nm with 100 fs pulse duration) [42–44]. To estimate the 2PA cross-section, one-photon excited PLQY was measured first. PLQY was measured against a standard, Rhodamine 6G in ethanol (PLQY ~ 0.9). PL spectra were measured using a Cary Eclipse spectrofluorometer (Varian Inc., Palo Alto, CA, USA). Absorption spectra were taken using a Shimadzu UV3600 spectrophotometer (Shimadzu corporation, Kyoto, Japan). PLQY was calculated using Equation (A4):

$$\varphi_s = \varphi_r \frac{I_s D_r}{I_r D_s} \left(\frac{n_r}{n_s} \right)^2, \quad (\text{A4})$$

where φ —one-photon excited PL quantum yield; I —PL spectra area, D —the optical density at the excitation wavelength, n —solution refractive index; indices r and s represent values for the reference and the sample, respectively.

Then, the 2PA cross-section was calculated using the Equation (A5):

$$\sigma_s^{2PA} \eta_s = \sigma_r^{2PA} \eta_r \frac{\varphi_r I_s^{2P} C_r n_r}{\varphi_s I_r^{2P} C_s n_s}, \quad (\text{A5})$$

where σ^{2PA} —2PA cross-section (in GM); φ —one-photon excited PLQY; η —two-photon excited PLQY; I^{2P} —two-photon excited PL spectra area, C —concentration (in M), n —solution refractive index; indices r and s represent values for the reference and the sample, respectively. Assuming that $\varphi = \eta$, the equation can be re-written as follows:

$$\sigma_s^{2PA} = \sigma_r^{2PA} \left(\frac{\varphi_r}{\varphi_s} \right)^2 \frac{I_s^{2P} C_r n_r}{I_r^{2P} C_s n_s}, \quad (\text{A6})$$

The 3PA absorption cross-section was calculated analogous to the 2PA cross-section with Rhodamine 6G in ethanol as a reference using the following equation:

$$\sigma_s^{3PA} = \sigma_r^{3PA} \left(\frac{\varphi_r}{\varphi_s} \right)^2 \frac{I_s^{3P} C_r n_r}{I_r^{3P} C_s n_s}, \quad (\text{A7})$$

where σ^{3PA} —3PA cross-section (in GM); φ —one-photon excited PLQY; I^{3P} —three-photon excited PL spectra area, C —concentration (in mol), n —solution refractive index; indices r and s represent values for the reference and the sample, respectively. The 3PA cross-section of Rhodamine 6G was taken as $3 \times 10^{-80} \text{ cm}^6 \text{ s}^2$ [45].

References

1. Kumawat, N.K.; Yuan, Z.; Bai, S.; Gao, F. Metal Doping/Alloying of Cesium Lead Halide Perovskite Nanocrystals and their Applications in Light-Emitting Diodes with Enhanced Efficiency and Stability. *Isr. J. Chem.* **2019**, *59*, 695–707. [[CrossRef](#)]
2. Xu, L.; Yuan, S.; Zeng, H.; Song, J. A comprehensive review of doping in perovskite nanocrystals/quantum dots: Evolution of structure, electronics, optics, and light-emitting diodes. *Mater. Today Nano* **2019**, *6*, 100036. [[CrossRef](#)]
3. Lu, C.-H.; Biesold-McGee, G.V.; Liu, Y.; Kang, Z.; Lin, Z. Doping and ion substitution in colloidal metal halide perovskite nanocrystals. *Chem. Soc. Rev.* **2020**, *49*, 4953–5007. [[CrossRef](#)]
4. Chen, Y.; Liu, Y.; Hong, M. Cation-doping matters in caesium lead halide perovskite nanocrystals: From physicochemical fundamentals to optoelectronic applications. *Nanoscale* **2020**, *12*, 12228–12248. [[CrossRef](#)]
5. Shen, X.; Zhang, Y.; Kershaw, S.V.; Li, T.; Wang, C.; Zhang, X.; Wang, W.; Li, D.; Wang, Y.; Lu, M.; et al. Zn-Alloyed CsPbI₃ Nanocrystals for Highly Efficient Perovskite Light-Emitting Devices. *Nano Lett.* **2019**, *19*, 1552–1559. [[CrossRef](#)]
6. Zhang, R.; Yuan, Y.; Li, J.; Qin, Z.; Zhang, Q.; Xiong, B.; Wang, Z.; Chen, F.; Du, X.; Yang, W. Ni and K ion doped CsPbX₃ NCs for the improvement of luminescence properties by a facile synthesis method in ambient air. *J. Lumin.* **2020**, *221*, 117044. [[CrossRef](#)]
7. Chen, J.-K.; Ma, J.-P.; Guo, S.-Q.; Chen, Y.-M.; Zhao, Q.; Zhang, B.-B.; Li, Z.-Y.; Zhou, Y.; Hou, J.; Kuroiwa, Y.; et al. High-Efficiency Violet-Emitting All-Inorganic Perovskite Nanocrystals Enabled by Alkaline-Earth Metal Passivation. *Chem. Mater.* **2019**, *31*, 3974–3983. [[CrossRef](#)]
8. Yong, Z.-J.; Guo, S.-Q.; Ma, J.-P.; Zhang, J.-Y.; Li, Z.-Y.; Chen, Y.-M.; Zhang, B.-B.; Zhou, Y.; Shu, J.; Gu, J.-L.; et al. Doping-Enhanced Short-Range Order of Perovskite Nanocrystals for Near-Unity Violet Luminescence Quantum Yield. *J. Am. Chem. Soc.* **2018**, *140*, 9942–9951. [[CrossRef](#)]
9. Pan, G.C.; Bai, X.; Xu, W.; Chen, X.; Zhai, Y.; Zhu, J.; Shao, H.; Ding, N.; Xu, L.; Dong, B.; et al. Bright Blue Light Emission of Ni²⁺ Ion-Doped CsPbCl_xBr_{3-x} Perovskite Quantum Dots Enabling Efficient Light-Emitting Devices. *ACS Appl. Mater. Interfaces* **2020**, *12*, 14195–14202. [[CrossRef](#)]
10. Chen, Y.-C.; Chou, H.-L.; Lin, J.-C.; Lee, Y.-C.; Pao, C.-W.; Chen, J.-L.; Chang, C.-C.; Chi, R.-Y.; Kuo, T.-R.; Lu, C.-W.; et al. Enhanced Luminescence and Stability of Cesium Lead Halide Perovskite CsPbX₃ Nanocrystals by Cu²⁺-Assisted Anion Exchange Reactions. *J. Phys. Chem. C* **2019**, *123*, 2353–2360. [[CrossRef](#)]
11. Van der Stam, W.; Geuchies, J.J.; Altantzis, T.; van den Bos, K.H.W.; Meeldijk, J.D.; Van Aert, S.; Bals, S.; Vanmaekelbergh, D.; De Mello Donega, C.D.M. Highly Emissive Divalent-Ion-Doped Colloidal CsPb_{1-x}MxB₃ Perovskite Nanocrystals through Cation Exchange. *J. Am. Chem. Soc.* **2017**, *139*, 4087–4097. [[CrossRef](#)]
12. Li, Y.; Zhang, X.; Huang, H.; Kershaw, S.V.; Rogach, A.L. Advances in metal halide perovskite nanocrystals: Synthetic strategies, growth mechanisms, and optoelectronic applications. *Mater. Today* **2020**, *32*, 204–221. [[CrossRef](#)]
13. Shamsi, J.; Urban, A.S.; Imran, M.; De Trizio, L.; Manna, L. Metal Halide Perovskite Nanocrystals: Synthesis, Post-Synthesis Modifications, and Their Optical Properties. *Chem. Rev.* **2019**, *119*, 3296–3348. [[CrossRef](#)]
14. Liu, M.; Grandhi, G.K.; Matta, S.; Mokurla, K.; Litvin, A.; Russo, S.; Vivo, P. Halide Perovskite Nanocrystal Emitters. *Adv. Photonics Res.* **2021**, *2*, 2000118. [[CrossRef](#)]
15. Yan, F.; Tan, S.T.; Li, X.; Demir, H.V. Light Generation in Lead Halide Perovskite Nanocrystals: LEDs, Color Converters, Lasers, and Other Applications. *Small* **2019**, *15*, e1902079. [[CrossRef](#)]
16. Gualdrón-Reyes, A.F.; Masi, S.; Mora-Seró, I. Progress in halide-perovskite nanocrystals with near-unity photoluminescence quantum yield. *Trends Chem.* **2021**, *3*, 499–511. [[CrossRef](#)]
17. Dey, A.; Ye, J.; De, A.; Debroye, E.; Ha, S.K.; Bladt, E.; Kshirsagar, A.S.; Wang, Z.; Yin, J.; Wang, Y.; et al. State of the Art and Prospects for Halide Perovskite Nanocrystals. *ACS Nano* **2021**, *15*, 10775–10981. [[CrossRef](#)]
18. Zou, S.; Liu, Y.; Li, J.; Liu, C.; Feng, R.; Jiang, F.; Li, Y.; Song, J.; Zeng, H.; Hong, M.; et al. Stabilizing Cesium Lead Halide Perovskite Lattice through Mn(II) Substitution for Air-Stable Light-Emitting Diodes. *J. Am. Chem. Soc.* **2017**, *139*, 11443–11450. [[CrossRef](#)]
19. Wang, H.-C.; Wang, W.; Tang, A.-C.; Tsai, H.-Y.; Bao, Z.; Ihara, T.; Yarita, N.; Tahara, H.; Kanemitsu, Y.; Chen, S.; et al. High-Performance CsPb_{1-x}SnxBr₃ Perovskite Quantum Dots for Light-Emitting Diodes. *Angew. Chem.* **2017**, *129*, 13838–13842. [[CrossRef](#)]
20. Yao, J.-S.; Ge, J.; Han, B.-N.; Wang, K.-H.; Yao, H.-B.; Yu, H.-L.; Li, J.-H.; Zhu, B.-S.; Song, J.-Z.; Chen, C.; et al. Ce³⁺-Doping to Modulate Photoluminescence Kinetics for Efficient CsPbBr₃ Nanocrystals Based Light-Emitting Diodes. *J. Am. Chem. Soc.* **2018**, *140*, 3626–3634. [[CrossRef](#)]
21. Todorović, P.; Ma, D.; Chen, B.; Quintero-Bermudez, R.; Saidaminov, M.I.; Dong, Y.; Lu, Z.; Sargent, E.H. Spectrally Tunable and Stable Electroluminescence Enabled by Rubidium Doping of CsPbBr₃ Nanocrystals. *Adv. Opt. Mater.* **2019**, *7*, 1470–1474. [[CrossRef](#)]
22. Yang, H.; Yin, W.; Dong, W.; Gao, L.; Tan, C.-H.; Li, W.; Zhang, X.; Zhang, J. Enhancing the light-emitting performance and stability in CsPbBr₃ perovskite quantum dots via simultaneous doping and surface passivation. *J. Mater. Chem. C* **2020**, *8*, 14439–14445. [[CrossRef](#)]
23. Hoang, M.T.; Pannu, A.S.; Tang, C.; Yang, Y.; Pham, N.D.; Gui, K.; Wang, X.; Yambem, S.; Sonar, P.; Du, A.; et al. Potassium Doping to Enhance Green Photoemission of Light-Emitting Diodes Based on CsPbBr₃ Perovskite Nanocrystals. *Adv. Opt. Mater.* **2020**, *8*, 2000742. [[CrossRef](#)]

24. Xu, J.; Li, X.; Xiong, J.; Yuan, C.; Semin, S.; Rasing, T.; Bu, X. Halide Perovskites for Nonlinear Optics. *Adv. Mater.* **2020**, *32*, e1806736. [[CrossRef](#)] [[PubMed](#)]
25. Denk, W.; Strickler, J.H.; Webb, W.W. Two-photon laser scanning fluorescence microscopy. *Science* **1990**, *248*, 73–76. [[CrossRef](#)]
26. Hell, S.W.; Bahlmann, K.; Schrader, M.; Soini, A.; Malak, H.M.; Gryczynski, I.; Lakowicz, J.R. Three-photon excitation in fluorescence microscopy. *J. Biomed. Opt.* **1996**, *1*, 71–74. [[CrossRef](#)]
27. Yu, J.H.; Kwon, S.-H.; Petrasek, Z.; Park, O.K.; Jun, S.W.; Shin, K.; Choi, M.; Park, Y.I.; Park, K.; Bin Na, H.; et al. High-resolution three-photon biomedical imaging using doped ZnS nanocrystals. *Nat. Mater.* **2013**, *12*, 359–366. [[CrossRef](#)]
28. Tong, L.; Cogley, C.M.; Chen, J.; Xia, Y.; Cheng, J.-X. Bright Three-Photon Luminescence from Gold/Silver Alloyed Nanostructures for Bioimaging with Negligible Photothermal Toxicity. *Angew. Chem. Int. Ed.* **2010**, *49*, 3485–3488. [[CrossRef](#)]
29. Chen, W.; Zhang, F.; Wang, C.; Jia, M.; Zhao, X.; Liu, Z.; Ge, Y.; Zhang, Y.; Zhang, H. Nonlinear Photonics Using Low-Dimensional Metal-Halide Perovskites: Recent Advances and Future Challenges. *Adv. Mater.* **2021**, *33*, 2004446. [[CrossRef](#)]
30. Shen, W.; Chen, J.; Wu, J.; Li, X.; Zeng, H. Nonlinear Optics in Lead Halide Perovskites: Mechanisms and Applications. *ACS Photonics* **2021**, *8*, 113–124. [[CrossRef](#)]
31. Ketavath, R.; Katturi, N.K.; Ghugal, S.G.; Kolli, H.K.; Swetha, T.; Soma, V.R.; Murali, B. Deciphering the Ultrafast Nonlinear Optical Properties and Dynamics of Pristine and Ni-Doped CsPbBr₃ Colloidal Two-Dimensional Nanocrystals. *J. Phys. Chem. Lett.* **2019**, *10*, 5577–5584. [[CrossRef](#)]
32. He, T.; Li, J.; Ren, C.; Xiao, S.; Li, Y.; Chen, R.; Lin, X. Strong two-photon absorption of Mn-doped CsPbCl₃ perovskite nanocrystals. *Appl. Phys. Lett.* **2017**, *111*, 211105. [[CrossRef](#)]
33. He, T.; Li, J.; Qiu, X.; Xiao, S.; Lin, X. Superior multiphoton absorption properties in colloidal Mn-doped CsPbCl₃ two-dimensional nanoplatelets. *Photonics Res.* **2018**, *6*, 1021–1027. [[CrossRef](#)]
34. Zhao, Y.; Shen, C.; Ding, L.; Liu, J.; Xiang, W.; Liang, X. Novel B-site Cd²⁺ doped CsPbBr₃ quantum dot glass toward strong fluorescence and high stability for wLED. *Opt. Mater.* **2020**, *107*, 110046. [[CrossRef](#)]
35. Mondal, N.; De, A.; Samanta, A. Achieving Near-Unity Photoluminescence Efficiency for Blue-Violet-Emitting Perovskite Nanocrystals. *ACS Energy Lett.* **2019**, *4*, 32–39. [[CrossRef](#)]
36. Xie, C.; Zhao, Y.; Shi, W.; Yang, P. Postsynthetic Surface-Treatment of CsPbX₃ (X = Cl, Br, or I) Nanocrystals via CdX₂ Precursor Solution toward High Photoluminescence Quantum Yield. *Langmuir* **2021**, *37*, 1183–1193. [[CrossRef](#)] [[PubMed](#)]
37. Parfenov, P.S.; Litvin, A.P.; Baranov, A.V.; Ushakova, E.V.; Fedorov, A.V.; Prudnikov, A.V.; Artemyev, M.V. Measurement of the luminescence decay times of PbS quantum dots in the near-IR spectral range. *Opt. Spectrosc.* **2012**, *112*, 868–873. [[CrossRef](#)]
38. Parfenov, P.S.; Litvin, A.P.; Ushakova, E.V.; Fedorov, A.V.; Baranov, A.V.; Berwick, K. Note: Near infrared spectral and transient measurements of PbS quantum dots luminescence. *Rev. Sci. Instrum.* **2013**, *84*, 116104. [[CrossRef](#)]
39. Skurlov, I.D.; Onishchuk, D.A.; Parfenov, P.S.; Litvin, A.P. An Experimental Setup for Analysis of Weak Photoluminescence in the Near-Infrared Spectral Region. *Opt. Spectrosc.* **2018**, *125*, 756–759. [[CrossRef](#)]
40. Han, Q.; Wu, W.; Liu, W.; Yang, Q.; Yang, Y. Temperature-dependent photoluminescence of CsPbX₃ nanocrystal films. *J. Lumin.* **2018**, *198*, 350–356. [[CrossRef](#)]
41. Das, A.; Arefina, I.A.; Danilov, D.V.; Koroleva, A.V.; Zhizhin, E.V.; Parfenov, P.S.; Kuznetsova, V.A.; Ismagilov, A.O.; Litvin, A.P.; Fedorov, A.V.; et al. Chiral carbon dots based on l/d-cysteine produced via room temperature surface modification and one-pot carbonization. *Nanoscale* **2021**, *13*, 8058–8066. [[CrossRef](#)]
42. Albota, M.A.; Xu, C.; Webb, W.W. Two-photon fluorescence excitation cross sections of biomolecular probes from 690 to 960 nm. *Appl. Opt.* **1998**, *37*, 7352–7356. [[CrossRef](#)]
43. Kapoor, R.; Friend, C.S.; Patra, A. Two-photon-excited absolute emission cross-sectional measurements calibrated with a luminance meter. *J. Opt. Soc. Am. B* **2003**, *20*, 1550–1554. [[CrossRef](#)]
44. Fischer, A.; Cremer, C.; Stelzer, E.H.K. Fluorescence of coumarins and xanthenes after two-photon absorption with a pulsed titanium-sapphire laser. *Appl. Opt.* **1995**, *34*, 1989–2003. [[CrossRef](#)]
45. Lanin, A.A.; Chebotarev, A.S.; Pochechuev, M.S.; Kelmanson, I.V.; Kotova, D.A.; Bilan, D.S.; Ermakova, Y.G.; Fedotov, A.B.; Ivanov, A.A.; Belousov, V.V.; et al. Two- and three-photon absorption cross-section characterization for high-brightness, cell-specific multiphoton fluorescence brain imaging. *J. Biophotonics* **2020**, *13*, e201900243. [[CrossRef](#)]
46. Navas, J.; Sánchez-Coronilla, A.; Gallardo, J.J.; Cruz Hernández, N.; Piñero, J.C.; Alcántara, R.; Fernández-Lorenzo, C.; De los Santos, D.M.; Aguilar, T.; Martín-Calleja, J. New insights into organic-inorganic hybrid perovskite CH₃NH₃PbI₃ nanoparticles. An experimental and theoretical study of doping in Pb²⁺ sites with Sn²⁺, Sr²⁺, Cd²⁺ and Ca²⁺. *Nanoscale* **2015**, *7*, 6216–6229. [[CrossRef](#)]
47. Cai, T.; Yang, H.; Hills-Kimball, K.; Song, J.-P.; Zhu, H.; Hofman, E.; Zheng, W.; Rubenstein, B.M.; Chen, O. Synthesis of All-Inorganic Cd-Doped CsPbCl₃ Perovskite Nanocrystals with Dual-Wavelength Emission. *J. Phys. Chem. Lett.* **2018**, *9*, 7079–7084. [[CrossRef](#)]
48. Varshni, Y.P. Temperature dependence of the energy gap in semiconductors. *Physica* **1967**, *34*, 149–154. [[CrossRef](#)]
49. Lee, W.; Li, H.; Wong, A.; Zhang, D.; Lai, M.; Yu, Y.; Kong, Q.; Lin, E.; Urban, J.J.; Grossman, J.C.; et al. Ultralow thermal conductivity in all-inorganic halide perovskites. *Proc. Natl. Acad. Sci. USA* **2017**, *114*, 8693–8697. [[CrossRef](#)]
50. Saran, R.; Heuer-Jungemann, A.; Kanaras, A.G.; Curry, R.J. Giant Bandgap Renormalization and Exciton-Phonon Scattering in Perovskite Nanocrystals. *Adv. Opt. Mater.* **2017**, *5*, 1700231. [[CrossRef](#)]

51. Li, J.; Yuan, X.; Jing, P.; Li, J.; Wei, M.; Hua, J.; Zhao, J.; Tian, L. Temperature-dependent photoluminescence of inorganic perovskite nanocrystal films. *RSC Adv.* **2016**, *6*, 78311–78316. [[CrossRef](#)]
52. Litvin, A.P.; Parfenov, P.S.; Ushakova, E.V.; Simões Gamboa, A.L.; Fedorov, A.V.; Baranov, A.V. Size and Temperature Dependencies of the Low-Energy Electronic Structure of PbS Quantum Dots. *J. Phys. Chem. C* **2014**, *118*, 20721–20726. [[CrossRef](#)]
53. Diroll, B.T.; Zhou, H.; Schaller, R.D. Low-Temperature Absorption, Photoluminescence, and Lifetime of CsPbX₃ (X = Cl, Br, I) Nanocrystals. *Adv. Funct. Mater.* **2018**, *28*, 1800945. [[CrossRef](#)]
54. Baranowski, M.; Plochocka, P. Excitons in Metal-Halide Perovskites. *Adv. Energy Mater.* **2020**, *10*, 1903659. [[CrossRef](#)]
55. Protesescu, L.; Yakunin, S.; Bodnarchuk, M.I.; Krieg, F.; Caputo, R.; Hendon, C.H.; Yang, R.X.; Walsh, A.; Kovalenko, M.V. Nanocrystals of Cesium Lead Halide Perovskites (CsPbX₃, X = Cl, Br, and I): Novel Optoelectronic Materials Showing Bright Emission with Wide Color Gamut. *Nano Lett.* **2015**, *15*, 3692–3696. [[CrossRef](#)]
56. Lu, M.; Zhang, Y.; Wang, S.; Guo, J.; Yu, W.W.; Rogach, A.L. Metal Halide Perovskite Light-Emitting Devices: Promising Technology for Next-Generation Displays. *Adv. Funct. Mater.* **2019**, *29*, 1902008. [[CrossRef](#)]
57. Van Le, Q.; Jang, H.W.; Kim, S.Y. Recent Advances toward High-Efficiency Halide Perovskite Light-Emitting Diodes: Review and Perspective. *Small Methods* **2018**, *2*, 1700419. [[CrossRef](#)]
58. Zhang, X.; Lin, H.; Huang, H.; Reckmeier, C.; Zhang, Y.; Choy, W.C.H.; Rogach, A.L. Enhancing the Brightness of Cesium Lead Halide Perovskite Nanocrystal Based Green Light-Emitting Devices through the Interface Engineering with Perfluorinated Ionomer. *Nano Lett.* **2016**, *16*, 1415–1420. [[CrossRef](#)]
59. Zhang, X.; Sun, C.; Zhang, Y.; Wu, H.; Ji, C.; Chuai, Y.; Wang, P.; Wen, S.; Zhang, C.; Yu, W.W. Bright Perovskite Nanocrystal Films for Efficient Light-Emitting Devices. *J. Phys. Chem. Lett.* **2016**, *7*, 4602–4610. [[CrossRef](#)]
60. He, G.S.; Tan, L.-S.; Zheng, A.Q.; Prasad, P.N. Multiphoton Absorbing Materials: Molecular Designs, Characterizations, and Applications. *Chem. Rev.* **2008**, *108*, 1245–1330. [[CrossRef](#)]
61. Ganeev, R.A.; Rao, K.S.; Yu, Z.; Yu, W.; Yao, C.; Fu, Y.; Zhang, K.; Guo, C. Strong nonlinear absorption in perovskite films. *Opt. Mater. Express* **2018**, *8*, 1472–1483. [[CrossRef](#)]
62. Liu, W.; Xing, J.; Zhao, J.; Wen, X.; Wang, K.; Lu, P.; Xiong, Q. Giant Two-Photon Absorption and Its Saturation in 2D Organic-Inorganic Perovskite. *Adv. Opt. Mater.* **2017**, *5*, 1601045. [[CrossRef](#)]
63. Pramanik, A.; Gates, K.; Gao, Y.; Begum, S.; Ray, P.C. Several Orders-of-Magnitude Enhancement of Multiphoton Absorption Property for CsPbX₃ Perovskite Quantum Dots by Manipulating Halide Stoichiometry. *J. Phys. Chem. C* **2019**, *123*, 5150–5156. [[CrossRef](#)]
64. Chen, J.; Židek, K.; Chábera, P.; Liu, D.; Cheng, P.; Nuuttila, L.; Al-Marri, M.J.; Lehtivuori, H.; Messing, M.E.; Han, K.; et al. Size- and Wavelength-Dependent Two-Photon Absorption Cross-Section of CsPbBr₃ Perovskite Quantum Dots. *J. Phys. Chem. Lett.* **2017**, *8*, 2316–2321. [[CrossRef](#)]
65. Krishnakanth, K.N.; Seth, S.; Samanta, A.; Rao, S.V. Broadband femtosecond nonlinear optical properties of CsPbBr₃ perovskite nanocrystals. *Opt. Lett.* **2018**, *43*, 603–606. [[CrossRef](#)] [[PubMed](#)]
66. Wang, Y.; Li, X.; Zhao, X.; Xiaoming, L.; Zeng, H.; Sun, H. Nonlinear Absorption and Low-Threshold Multiphoton Pumped Stimulated Emission from All-Inorganic Perovskite Nanocrystals. *Nano Lett.* **2015**, *16*, 448–453. [[CrossRef](#)]
67. Han, Q.; Wu, W.; Liu, W.; Yang, Q.; Yang, Y. Two-photon absorption and upconversion luminescence of colloidal CsPbX₃ quantum dots. *Opt. Mater.* **2018**, *75*, 880–886. [[CrossRef](#)]
68. He, T.; Li, J.; Qiu, X.; Xiao, S.; Yin, C.; Lin, X. Highly Enhanced Normalized-Volume Multiphoton Absorption in CsPbBr₃ 2D Nanoplates. *Adv. Opt. Mater.* **2018**, *6*, 1800843. [[CrossRef](#)]
69. Xu, Y.; Chen, Q.; Zhang, C.; Wang, R.; Wu, H.; Zhang, X.; Xing, G.; Yu, W.W.; Wang, X.; Zhang, Y.; et al. Two-Photon-Pumped Perovskite Semiconductor Nanocrystal Lasers. *J. Am. Chem. Soc.* **2016**, *138*, 3761–3768. [[CrossRef](#)]
70. Chen, W.; Bhaumik, S.; Veldhuis, S.A.; Xing, G.; Xu, Q.; Grätzel, M.; Mhaisalkar, S.; Mathews, N.; Sum, T.C. Giant five-photon absorption from multidimensional core-shell halide perovskite colloidal nanocrystals. *Nat. Commun.* **2017**, *8*, 15198. [[CrossRef](#)] [[PubMed](#)]
71. Li, M.; Bhaumik, S.; Goh, T.W.; Kumar, M.S.; Yantara, N.; Grätzel, M.; Mhaisalkar, S.; Mathews, N.; Sum, T.C. Slow cooling and highly efficient extraction of hot carriers in colloidal perovskite nanocrystals. *Nat. Commun.* **2017**, *8*, 14350. [[CrossRef](#)] [[PubMed](#)]
72. Li, J.; Jing, Q.; Xiao, S.; Gao, Y.; Wang, Y.; Zhang, W.; Sun, X.W.; Wang, K.; He, T. Spectral Dynamics and Multiphoton Absorption Properties of All-Inorganic Perovskite Nanorods. *J. Phys. Chem. Lett.* **2020**, *11*, 4817–4825. [[CrossRef](#)] [[PubMed](#)]
73. Pramanik, A.; Patibandla, S.; Gao, Y.; Gates, K.; Ray, P.C. Water Triggered Synthesis of Highly Stable and Biocompatible 1D Nanowire, 2D Nanoplatelet, and 3D Nanocube CsPbBr₃ Perovskites for Multicolor Two-Photon Cell Imaging. *JACS Au* **2021**, *1*, 53–65. [[CrossRef](#)]
74. Catalano, I.M.; Cingolani, A. Three-photon absorption coefficient determination by means of nonlinear luminescence experiments. *J. Appl. Phys.* **1979**, *50*, 5638–5641. [[CrossRef](#)]
75. Maes, J.; Balcaen, L.; Drijvers, E.; Zhao, Q.; De Roo, J.; Vantomme, A.; Vanhaecke, F.; Geiregat, P.; Hens, Z. Light Absorption Coefficient of CsPbBr₃ Perovskite Nanocrystals. *J. Phys. Chem. Lett.* **2018**, *9*, 3093–3097. [[CrossRef](#)]
76. Wang, Y.; Li, X.; Song, J.; Xiaoming, L.; Zeng, H.; Sun, H. All-Inorganic Colloidal Perovskite Quantum Dots: A New Class of Lasing Materials with Favorable Characteristics. *Adv. Mater.* **2015**, *27*, 7101–7108. [[CrossRef](#)]
77. Makarov, N.S.; Guo, S.; Isaienko, O.; Liu, W.; Robel, I.; Klimov, V.I. Spectral and Dynamical Properties of Single Excitons, Biexcitons, and Triions in Cesium-Lead-Halide Perovskite Quantum Dots. *Nano Lett.* **2016**, *16*, 2349–2362. [[CrossRef](#)] [[PubMed](#)]

78. Zhang, F.; Liu, Y.; Wei, S.; Chen, J.; Zhou, Y.; He, R.; Pullerits, T.; Zheng, K. Microscopic morphology independence in linear absorption cross-section of CsPbBr₃ nanocrystals. *Sci. China Mater.* **2021**, *64*, 1418–1426. [[CrossRef](#)]
79. Puthenpurayil, J.; Cheng, O.H.-C.; Qiao, T.; Rossi, D.; Son, D.H. On the determination of absorption cross section of colloidal lead halide perovskite quantum dots. *J. Chem. Phys.* **2019**, *151*, 154706. [[CrossRef](#)]
80. Beaumont, P.C.; Johnson, D.G.; Parsons, B.J. Photophysical properties of laser dyes: Picosecond laser flash photolysis studies of Rhodamine 6G, Rhodamine B and Rhodamine 101. *J. Chem. Soc. Faraday Trans.* **1993**, *89*, 4185–4191. [[CrossRef](#)]
81. Dempster, D.N.; Morrow, T.; Quinn, M.F. The photochemical characteristics of rhodamine 6G-ethanol solutions. *J. Photochem.* **1973**, *2*, 343–359. [[CrossRef](#)]